Hepatitis B Virus–Mediated m6A Demethylation Increases Hepatocellular Carcinoma Stemness and Immune Escape

Yuting Meng[1], Zheyue Shu[2], Xueyao Wang[3], Liang Hong[1], Baohua Wang[4], Jingjing Jiang[1], Kangxin He[1,2], Qingyi Cao[1], Fan Shi[1], Hai Wang[5], Lan Gong[6], and Hongyan Diao[1]

ABSTRACT

Hepatitis B viral (HBV) persistent infection plays a significant role in hepatocellular carcinoma (HCC) tumorigenesis. Many studies have revealed the pivotal roles of N6-methyladenosine (m6A) in multiple cancers, while the regulatory mechanism in stemness maintenance of HBV persistent infection-related HCC remains elusive. Here, we demonstrated that the level of m6A modification was downregulated by HBV in HBV-positive HCC, through enhanced stability of ALKBH5 mRNA. More specifically, we also identified that ALKBH5 mRNA was functionally required for the stemness maintenance and self-renewal in the HBV-positive HCC, but dispensable in HBV-negative HCC. Mechanistically, ALKBH5 demethylated the m6A modification in the 3′ untranslated region of the oncogenic gene *SNAI2* to prevent the recognition of YTHDF2 therewith stabilize *SNAI2* transcripts, contributing to cancer stem cell traits in HBV-positive HCC. Moreover, the expression of *SNAI2* reversed the suppression of stemness properties by knocking down ALKBH5. In addition, ALKBH5/SNAI2 axis accelerates tumor immune evasion through activated ligand of immune checkpoint CD155. Our study unveiled that the ALKBH5 induces m6A demethylation of the *SNAI2* as a key regulator in HBV-related HCC, and identifies the function of ALKBH5/SNAI2/YTHDF2 axis in promoting the stem-like cells phenotype and immune escape during HBV infection.

Implications: HBV promotes HCC stemness maintenance through elevate m6A modification of SNAI2 in an ALKBH5-YTHDF2–dependent manner and increases the expression of the ligand of immune checkpoint CD155.

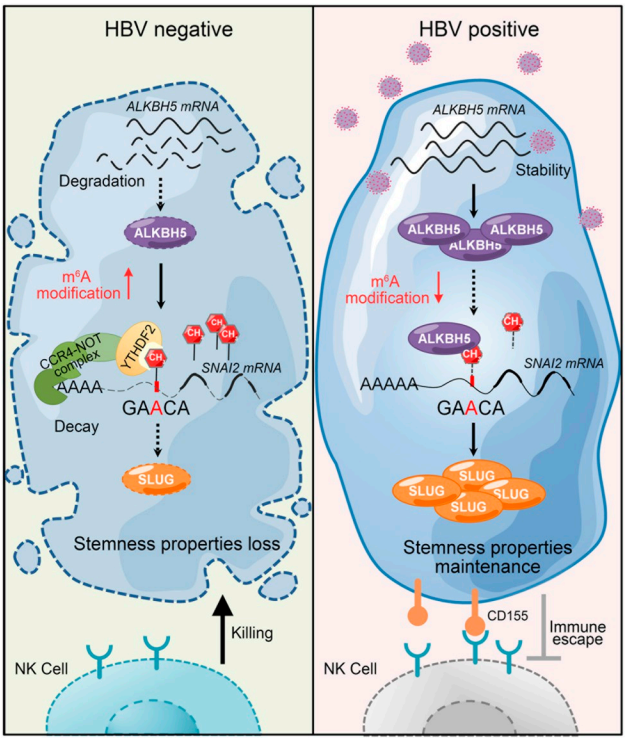

Introduction

The hepatocellular carcinoma (HCC) as one of the common malignancies is the fourth leading cause of tumor lethal disease worldwide (1, 2). Hepatitis B viral (HBV) infection has been defined as a major risk factor of HCC (3–5). Thus, clarifying the molecular mechanisms and developing the biomarkers of HBV-related HCC are essential to prove clinical diagnostics and benefit to precise treatment.

Accumulated studies revealed that cancer stem cells (CSC) maintained in HCC is the root cause of recurrence, therapy resistance, and immune escape (6–8). HBV as the major predisposing factors for HCC has been known to trigger HCC malignancy and

[1]State Key Laboratory for Diagnosis and Treatment of Infectious Diseases, National Clinical Research Center for Infectious Diseases, National Medical Center for Infectious Diseases, Collaborative Innovation Center for Diagnosis and Treatment of Infectious Diseases, The First Affiliated Hospital, Zhejiang University School of Medicine, Hangzhou, Zhejiang, P.R. China. [2]Division of Hepatobiliary and Pancreatic Surgery, Department of Surgery, The First Affiliated Hospital, Zhejiang University School of Medicine, Hangzhou, Zhejiang, P.R. China. [3]Jinan Microecological Biomedicine Shandong Laboratory, Jinan, Shandong, P.R. China. [4]Department of Ultrasound, The First Affiliated Hospital, College of Medicine, Zhejiang University, Hangzhou, Zhejiang Province, P.R. China. [5]Department of Laboratory, Tongde Hospital of Zhejiang Province, Hangzhou, Zhejiang, P.R. China. [6]Microbiome Research Centre, St George and Sutherland Clinical School, University of New South Wales, Sydney, New South Wales, Australia.

Corresponding Author: Hongyan Diao, State Key Laboratory for Diagnosis and Treatment of Infectious Diseases, National Clinical Research Center for Infectious Diseases, National Medical Center for Infectious Diseases, Collaborative Inn, The First Affiliated Hospital, Zhejiang University, Hangzhou 310000, Zhejiang, P.R. China. E-mail: diaohy@zju.edu.cn

Mol Cancer Res 2024;22:642–55

doi: 10.1158/1541-7786.MCR-23-0720

promote the progression of HCC though multiple pathways (9, 10). A recent study found that HBV contributes to liver cancer stemness. In addition, HBV was reported to elevate the expression of EpCAM by promoting DNA demethylation (11, 12). However, the mechanism of RNA epigenetic modifications conferring CSC features to HBV-related HCC remains an incomplete story.

N6-methyladenosine (m6A) has been reported to participate in many human cancers including HCC (13). Recently, METTL3 was shown to be an oncogenic factor in glioblastoma tumor, acute myeloid leukemia, and promotes hematopoietic stem cell maintenance (14–16). FTO has been reported to enhance leukemogenesis and suppress leukemia cell differentiation (17, 18). These findings suggested the modulatory functional importance of m6A modification in the progression of cancer development and CSC properties.

In this study, HBV tilt down the m6A modification level through stabilizing the mRNA of ALKBH5. Moreover, the reduced m6A modification of oncogenic *SNAI2* significantly enhanced the stabilization of *SNAI2* mRNA and promoted the stem-like cell features. In addition, *SNAI2* gene reversed the suppression of CSC properties and immune checkpoint response which was alleviated by knocking down ALKBH5 in HBV-related HCC. Taken together, our study unveiled that HBV promotes the stem-like cell phenotype and immune escape via the ALKBH5/*SNAI2*/YTHDF2 axis.

Materials and Methods

Cell culture and tissue specimens

Liver tissues were collected from patients with HCC who were recruited from the patients underwent surgical resection, following written informed consent from patients and approved by the Institutional Ethics Review Board of First Affiliated Hospital of Zhejiang University (Hangzhou, Zhejiang, P.R. China). All studies were conducted in accordance with the Declaration of Helsinki. The patients with HCC were without any other viral infections. The study focused on patients with HCC without any other viral infections including viral hepatitis caused by virus other than HBV (such as HAV, HCV, HEV) were excluded from the study. Two groups of tumor specimens with similar age and sex distributions were recognized to be histologically normal by two independent pathologists.

The human liver cancer cell lines were obtained from the State Key Laboratory for Diagnosis and Treatment of Infectious Diseases, The First Affiliated Hospital, Zhejiang University. Mouse Hepa1-6 cell line was purchased from Shanghai Cell Bank (Chinese Academy of Sciences, Shanghai, P.R. China). These cells were cultured in DMEM (Gibco, 10569044) containing 10% FBS (Gibco, 10100147). The human NK-92MI cells were purchased from ATCC. NK-92MI cells were maintained in MEMα (Invitrogen) supplemented with 12.5% FBS (Gibco), 12.5% horse serum (Gibco), 0.2 mmol/L inositol, 0.1 mmol/L β-mercaptoethanol, 0.02 mmol/L folic acid, and 1% penicillin/streptomycin. All cell lines used were cultured within 10 generations after thawing and tested negative for *Mycoplasma* throughout the study. The identities of cell lines were verified using the short tandem repeat (STR) profiling.

All cells were maintained at 37°C in a 5% CO_2 atmosphere and were not cultured continuously for more than 2 months. Cells were authenticated using STR analysis.

Xenograft in nude mice

Six-week-old female BALB/c nude mice were purchased from the Shanghai SLAC Laboratory Animal Co. Ltd. Hep3B cells and HepG2.215 cells with stable ALKBH5 knockdown and SLUG overexpression were harvested and suspended in DMEM, and 1×10^7 stable cells in 100 μL of PBS were subcutaneously injected into the armpit of nude mice ($n = 7$ each group). The tumor size was measured using calipers. After 4 weeks, the nude mice were sacrificed and the growth of subcutaneous tumors was measured.

All animal studies were approved by the Institute Animal Care Commission of Zhejiang University (Hangzhou, Zhejiang, P.R. China) and carried out in accordance with established institutional guidelines and approved protocols.

Western blot analysis

Cells were lysed using RIPA buffer with 1% cocktail (Sigma, P2714) for 15 minutes. After centrifugation, the supernatant was collected and boiled with 5× loading buffer. Equal amounts of proteins were loaded and separated by SDS-PAGE, transferred to nitrocellulose membranes (Millipore, HATF00010). The membranes were incubated with primary and secondary antibodies and subsequently incubated using WesternBright ECL kit for chemiluminescent reading on Bio-Rad Gel-Doc System. Antibodies used for Western blot analysis are as follow: β-Catenin (8480) and GAPDH (5174) were purchased from Cell Signaling Technology. Nanog (ab109250), Oct-4 (ab200834), c-Myc (ab32072), CD133 (ab216323), CD34 (ab81289), β-actin (ab8227), YTHDF2 (ab220163), and SLUG (ab27568) were purchased from Abcam. ALKBH5 (16837-1-AP) was purchased from Proteintech.

Sphere formation assay

Sphere formation was done as our previously reported with minor change (19). In brief, cells were seeded in 6-well ultralow attachment plates (Corning, 3471) at a density of 1×10^3 cells per well with sphere medium and add medium once every 2 days. Sphere medium includes DMEM/F12 (Gibco, C11330500BT), 20 ng/mL basic FGF (Petrotech, 100-18B), 20 μL/mL B27 (Thermo Fisher Scientific, 17504044), and 20 ng/mL EGF (Petrotech, 100-05). After 14 days, the number and diameter of tumor spheres were calculated with the inverted microscope (Olympus, DP73). The sphere spheroids with independent three-dimensional structures (diameter greater than 50 μm) were measured and counted under Olympus microscope.

For replanting sphere formation, cells were seeded as above protocol, then, cells were digested with 2.5% trypsin and replanted into 6-well ultralow attachment plates at a density of 1×10^3 cells per well. The number and diameter of spheres were calculated after 14 days.

Multiplex IHC and quantitative analysis

The tissue microarray (TMA) sections were stained with multiplex fluorescence by using the Multiplex Fluorescent Immunostaining Kit (Absin). After deparaffinized in xylene and rehydrated in 100%, 90%, 70% alcohol successively. Antigen unmasking was performed with a preheated epitope retrieval solution. Next, the sections were incubated overnight with primary antibodies: anti c-Myc (ab32072), anti-m6A rabbit, anti ALKBH5 (16837-1-AP). Next, sections were incubated with secondary antibody for 20 minutes at room temperature. At last, 4′, 6-diamidino-2-phenylindole (DAPI; F6057, Sigma) was used to stain the nuclei and seal the slides. Imaging was achieved using the Case Viewer2.4 (3DHISTECH) and analysis using AIpathwell (Servicebio). The area density for each sample was calculated in the following way: integrated option density/tissue area, pixel. The ROC curve analysis was used to select the cut-off point for each variable.

Establishing HCC organoids

HCC tissues were isolated from patient with HCC then rinsed with cold Dulbecco's phosphate buffered saline (DPBS) and minced into 0.2 mm^3 pieces. Tissue fragments were then digested with collagenase IV supplemented with DNAse I (Sigma) at 37°C for 1 hour. DMED supplemented with 10% FBS was added into tissues after digestion. Repetitive the tissues in cold DPBS and filtered cells using a 70 μm cell strainer (Corning), then washing in DPBS for two times. The cells were counted and mixed with Matrigel (Corning) and seeded into 48-well plates. Cells were incubated with organoids culture medium (Absin).

MeRIP-seq data analysis

m6A methylated RNA immunoprecipitation sequencing (MeRIP-seq) data are with the following accession numbers: GSE155657 and GSE179680. All data were aligned to the corresponding reference genome and visualized using IGV: Integrative Genomics Viewer (http://www.broadinstitute.org/igv).

NK-92MI cell killing assay

The xCELLigence real-time cellular analysis (RTCA) instrument (ACEA Biosciences) was utilized for cell killing experiments. First, 50 μL of target cell culturing media (DMEM+10% FBS) was added to each well of 96-well E-Plates (ACEA Biosciences) and the background impedance was measured and displayed as Cell Index. Then Hep3B or HepG2.215 cells were seeded at a density of 10,000 (HepG2.215) or 8,000 (Hep3B) cells/well of the E-Plate in a volume of 50 μL and allowed to adhere on the electrode surface. Post seeding, transferred NK-92 cell in target ratios (10:1) to the RTCA MP instrument inside a cell culture incubator. Data recording was initiated immediately at 10-minute intervals for the entire duration of the experiment. For each well, the % Cell viability utilizes the Normalized Sample Cell Index Control.

IHC and scoring

Tissue sections for IHC staining were deparaffinized, rehydrated and antigen retrieved and then blocked with blocking buffer (5% goat serum, 0.1% Triton X-100 in PBS) for 1 hour at room temperature. The slides were incubated with anti-ALKBH5 (Proteintech, 16837-1-AP), anti-SLUG (Abcam, ab27568) or anti-m6A primary antibody (Synaptic Systems) at 4°C overnight and washed three times with PBS for 20 minutes each wash, followed by incubation with biotin-labeled corresponding secondary antibody. Scoring was performed using Image J software. Typical images corresponding to High positive (scored as "3"), Positive (score as "2"), Low positive (score as "1"), and Negative (score as "0") brown staining were selected by two independent pathologist for software training. The H-score for each sample was calculated according to the following formula: (% of cells stained at intensity 1*1) þ (% of cells stained at intensity 2 * 2) þ (% of cells stained at intensity 3 * 3).

Statistical analysis

Statistical analyses were carried out using GraphPad Prism (version 8.0; GraphPad Inc.) and R (version 3.6) software for Windows. Statistical comparisons were performed by using Student *t* test (two-tailed unpaired), ANOVA test or Bonferroni test as indicated in the figure legends. Statistical analysis for correlation was performed using two-tailed Pearson correlation test. A P value of <0.05 was considered statistically significant.

Data availability

Data supporting the current study are available from the corresponding author upon reasonable request.

Results

Reduced m6A levels in HBV-positive HCC cells enhance stemness maintenance

To investigate the variations of m6A modification in mRNAs of HCC, the m6A level was detected in 20 cases of tumor from patients with HCC. The level of m6A was significantly downregulated in HBV-positive HCC tissues with IHC staining and the representative images of IHC were shown (**Fig. 1A**). The m6A quantification was also showed decreased m6A modification in HBV-positive HCC tissues compared with HBV-negative HCC (**Fig. 1B**). Because of the hypomethylation that has been reported to promote the tumorigenesis and stemness of breast cancer (20), we then performed multicolor IHC (mIHC) staining of m6A and stem cell marker c-MYC in TMA to determine their associations in HCC tissues. The expression of m6A was negatively correlated with the expression of c-MYC in HBV-positive HCC tissues (**Fig. 1C**). The expression of reprogramming genes NANOG, OCT4 and liver CSC-related surface marker CD133, CD44 (21–23) significantly increased in HBV-positive HCC tissues compared with HBV-negative HCC (Supplementary Fig. S1A). Meanwhile, we further measured the m6A levels in HBV-negative HCC cell line HepG2 and HepG2 cell line infected with HBV from HepG2.215 supernatant or transfected with HBV plasmid, and the result showed that the HBV-positive cells have a decline of m6A modification compared with HBV-negative ones (Supplementary Fig. S1B). We performed sphere formation assay to detect the stemness traits of hepatoma cell lines. HBV-positive cell lines HepG2.215 and Hep3B showed significantly increased diameter and number of spheres compared with HBV-negative cell lines HepG2 and Huh7, respectively (**Fig. 1D**). Moreover, the expression of stem cell markers *MYC*, *NANOG*, *SOX2*, *POU5F1* were also elevated in HBV-positive cell lines (HepG2.215 and Hep3B) sphere compared with HBV-negative cell lines (HepG2 and Huh7), respectively (Supplementary Fig. S1C). Taken together, our data indicated that the total m6A levels in mRNA may regulate the stemness maintenance of HBV-related HCC cells.

HBV enhances *ALKBH5* mRNA stability to promote stem cell–like properties

We further explored the key regulators of m6A that contribute to the stemness maintenance via m6A-dependent manner in HBV-positive HCC. As the level of m6A modification is mainly regulated by methylases and demethylases, we measured the expression of "writer" proteins including METTL3, METTL14, WTAP, and "eraser" proteins including ALKBH5, FTO in HCC tissues. The expression levels of m6A regulators were different in HBV-negative cell line and HBV-positive cell line, among which, ALKBH5 with the most significant increase in HBV-positive cell line (Supplementary Fig. S2A). Compared with HBV-negative HCC, the mRNA level and protein expression of ALKBH5 were both significantly enriched in HBV-positive specimens (**Fig. 2A–C**). In addition, a significant upregulation of ALKBH5 was associated with the enrichment of CD133 and CD44 in HBV-positive HCC cell line and the expression of ALKBH5 was elevated in hepatoma CSC-enriched spheroids (**Fig. 2D**; Supplementary Fig. S2B). We next investigated the regulation of HBV in ALKBH5 expression using the cell model as our previous study described (24, 25). Both transfection with HBV plasmid and infection with HBV supernatant could elevate the mRNA level and protein expression of ALKBH5 in HBV-negative cell line (**Fig. 2E**; Supplementary Fig. S2C). In addition, the overexpression of ALKBH5 can lead to the downregulation of m6A level, while the mutant-type ALKBH5 overexpression cannot, and the knockdown of ALKBH5 led to the increased m6A level, indicating

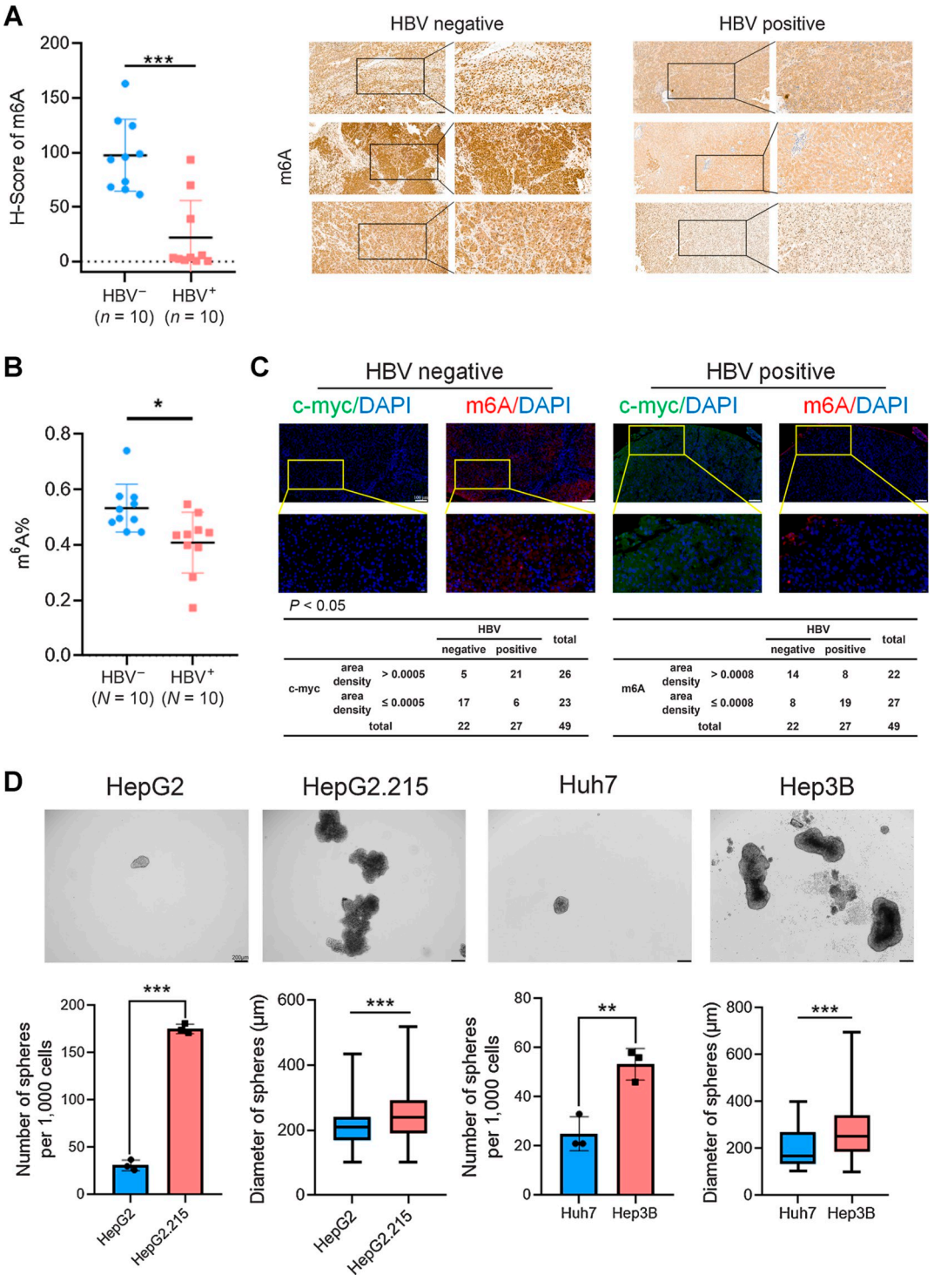

Figure 1.

Reduced m6A levels in HBV-positive HCC cells enhance stemness maintenance. Expression of m6A in HCC tissues was detected by IHC (**A**) and m6A quantification (**B**). Scale bar, 100 or 50 μm. **C,** Representative images of m6A, c-MYC mIHC staining in HCC tumor specimens with DAPI staining. Magnification: 15× or 40×. **D,** Sphere formation was performed in cell lines HepG2, HepG2.215, Huh7, Hep3B. Scale bar, 200 μm. The diameter and number of spheres from each experiment were represented as the mean ± SD and statistically analyzed; $n = 3$; *, $P < 0.05$; **, $P < 0.01$; ***, $P < 0.001$.

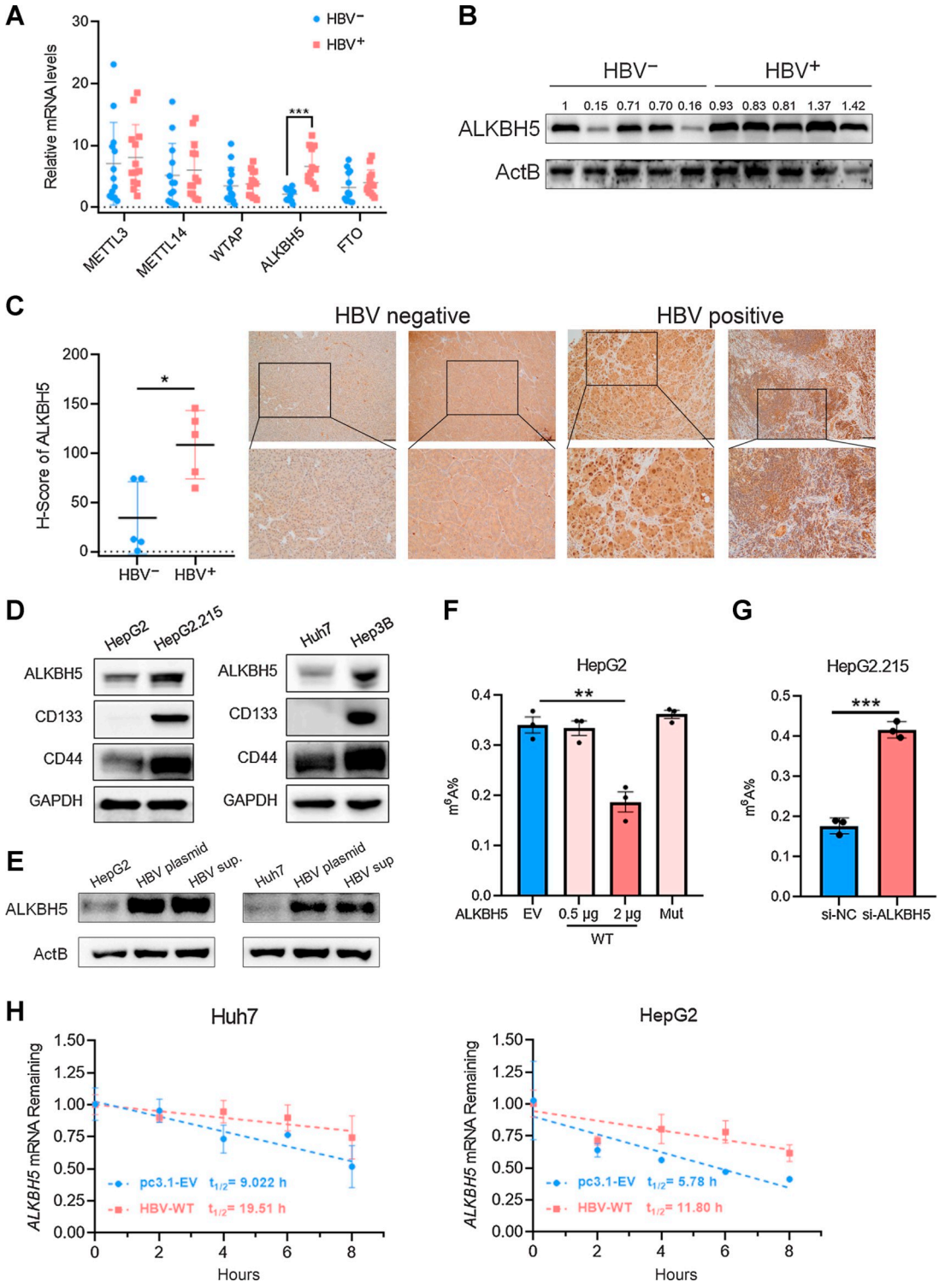

Figure 2.

HBV enhances *ALKBH5* mRNA stability to promote stem cell–like properties. **A** and **B,** The mRNA and protein expression of indicated m6A regulators were detected in HCC tissues. **C,** IHC analysis and representative images of ALKBH5 IHC staining in HBV-positive HCC and HBV-negative HCC specimens. Scale bar, 100 or 50 μm. **D,** The protein expression of ALKBH5, CD133, and CD44 in HepG2, HepG2.215, Huh7, and Hep3B cells. **E,** Relative protein levels of ALKBH5 were determined between HepG2 and Huh7 cells stimulated with HBV supernatant or transfected with HBV plasmid compared with cell line control. **F** and **G,** m6A abundance was detected in HepG2 transfected with ALKBH5 (wide type: WT) and ALKBH5 (active site mutant type: Mut) and in HepG2.215 transfected with siRNA segment target to ALKBH5. **H,** Stability of ALKBH5 mRNA in HepG2 and Huh7 cells transfected with HBV plasmid and empty vector were quantified by qRT-PCR after stimulated with ActD for 0, 2, 4, 6, 8 hours; $n = 3$; *, $P < 0.05$; **, $P < 0.01$; ***, $P < 0.001$.

that the change of ALKBH5 in HCC cell model can directly lead to the disorder of m6A (**Fig. 2F** and **G**). We next explored how HBV upregulates ALKBH5 expression. We cotransfected HBV-negative cell line HepG2 with the plasmids expressing HBV and HBV proteins HBp, HBs, HBc, HBx. The result showed that HBV plasmid could markedly increase the expression of ALKBH5 and induced the elevation of stem cell markers compared with other HBV proteins (Supplementary Fig. S2D and S2E). Then, *ALKBH5* mRNA expression was evaluated in both empty vector (EV) control and HBV-overexpression cells treated with cycloheximide and actinomycin D (ActD). The data showed no difference between the synthesis of *ALKBH5* in two groups (Supplementary Fig. S2F) while the half-life of *ALKBH5* mRNA being significantly longer upon HBV expression in the presence of ActD (**Fig. 2H**). Thus, these findings demonstrated that HBV enhances *ALKBH5* mRNA stability and expression of CSC markers, which indicating ALKBH5 may play a crucial role in stemness maintenance of HBV-positive HCC.

ALKBH5 is required for the maintenance of hepatoma cell self-renewal in HBV-positive HCC

We next investigated the potential mechanism of ALKBH5 oncogenic function in HBV-positive HCC. The expression levels of liver cancer stemness–related factors CD133 and CD44 were significantly decreased in ALKBH5 knockdown cells and elevated in ALKBH5 wild-type (WT) overexpression cells but not in enzyme-inactivated type (Mut) in HBV-positive cells (**Fig. 3A**; Supplementary Fig. S3A and S2B). In addition, the expression of well-known CSC markers *MYC*, *NANOG*, *SOX2*, *POU5F1* were also alleviated by ALKBH5 transient knockdown in Hep3B and HepG2.215 cells (Supplementary Fig. S3C and S3D). Subsequently, we construct the stable ALKBH5-knockdown cell line shALKBH5 (Supplementary Fig. S3E) and confirmed the enhanced m6A modification (Supplementary Fig. S3F). CSC markers were not decreased by knockdown ALKBH5 in HBV-negative cell lines (Supplementary Fig. S3G). Colony formation assay was performed, and the results showed a significant reduction of colony number in ALKBH5-depleted cells (**Fig. 3B**; Supplementary Fig. S3H). Sphere formation assay showed that ALKBH5 knockdown observably decreased the diameter and number of spheres in HBV-positive cell lines Hep3B and HepG2.215 but not in HBV-negative cell lines Huh7 and HepG2 (**Fig. 3C–E**; Supplementary Fig. S3I). Consistently, ALKBH5 depletion substantially alleviated the tumor transplantation ability in Hep3B (**Fig. 3F** and **G**) and HepG2.215 (Supplementary Fig. S3J) using extreme limiting dilution assays. Next, we tested the oncogenic effect of ALKBH5 *in vivo* by injecting the stable ALKBH5-depleted Hep3B cells (shALKBH5) or control cells (shNC) into nude mice. Mice inoculated with ALKBH5-deficient cells evidently formed smaller tumor masses than the mice injected with control cells (**Fig. 3H–J**). These results collectively revealed that ALKBH5 is crucial for tumor growth and tumorigenic ability in HBV-positive HCC.

SNAI2 is a functionally important target gene of ALKBH5 in HBV-positive HCC

To assess the biological function and potential target genes of ALKBH5 in HBV-positive HCC, we first employed MeRIP-seq to analyze the altered gene expression and m6A distribution in control (shNC) cells and ALKBH5 knockdown (shALK) cells with two independent biological replicates. The RRACH (R: G > C > U, H: C > U > A) motif was identified to be highly enriched within m6A sites in ALKBH5-deficeint cells (**Fig. 4A**). Next, we mapped the m6A distribution patterns of both groups in different mRNA regions. Importantly, the m6A peak abundance in 3′ untranslated regions (UTR) was relatively increased from 22.4% to 34.3% in ALKBH5-deficient cells compared with control cells (**Fig. 4B**). The result of m6A peak frequency distribution on mRNA was presented a consistent pattern (**Fig. 4C**). We analyzed the m6A enrichment peak in m6A-seq and mapped to corresponding genes (**Fig. 4D**) and comprehensively analyzed the MeRIP-seq and RNA sequencing (RNA-seq) data. We identified 672 transcripts with downregulated expression and enriched abundance m6A modification (**Fig. 4E**). Then we focused on the top 10 genes from overlap and listed them in ascending order of m6A methylation fold change (**Fig. 4F**; Supplementary Fig. S4A). Of these 10 genes, *SNAI2* (Snail family transcriptional repressor 2, protein name is SLUG) showed remarkably decrease in HBV-positive stable lines (Supplementary Fig. S4B) and *SNAI2* has long been reported to be an oncogene and promote the progression of invasion and stem cell–like maintenance in cancer cells (26, 27). Furthermore, depletion of ALKBH5 decreased the mRNA and protein levels of *SNAI2*, respectively (**Fig. 4G** and **H**). We next detect the mRNA levels of *ALKBH5* and *SNAI2* in HCC patient tissues, the expression of ALKBH5 was positively correlated to the expression of SNAI2 in patients' sample (**Fig. 4I**). These results suggested *SNAI2* as a functionally important target gene of ALKBH5 in HBV-positive HCC, and our following research focused on this gene.

ALKBH5-mediated m6A demethylation in 3′ UTR stabilizes *SNAI2* mRNA via an YTHDF2-dependent pathway

Because *SNAI2* could be a direct target gene of ALKBH5, we investigated the precisely regulatory mechanism of SLUG (protein name of *SNAI2*) by ALKBH5. By analyzing the MeRIP-seq data, we found two high-confidence m6A peaks distributed in the 3′ UTR (P1) and the CDS region (P2) of *SNAI2* mRNA, respectively, including three putative m6A sites (**Fig. 5A**; Supplementary Fig. S4A). MeRIP-qPCR was performed to confirm the location of ALKBH5-mediated m6A demethylation of *SNAI2* using specific primer of each peak region. The m6A deposition accumulated in the 3′ UTR of *SNAI2* mRNA was obtained in ALKBH5-deficent cells compared with control cells (**Fig. 5B**; Supplementary Fig. S4C and S4D). We next detected the "reader" that recognizes the P1 region of *SNAI2* mRNA and found that the mRNA level of *SNAI2* was upregulated with YTHDF2-knockdown, but not with other reader's knockdown (**Fig. 5C**; Supplementary Fig. S4E). The protein level of SLUG was consistent with the previous mRNA result in YTHDF2-deficent cells (**Fig. 5D**). In addition, YTHDF2 transient knockdown (siYTHDF2) also rescued the mRNA and protein expression of *SNAI2* in the endogenous stable ALKBH5-knockdown cell line (**Fig. 5E** and **F**). Several studies have reported that YTHDF2 brings mRNAs with m6A modification to mRNA decay sites and subsequently recruits CCR4–NOT complex to trigger deadenylation in 3′ UTR leading to degradation of the transcripts (28). In our study, we found that ablation of YTHDF2 (siYTHDF2) significantly extended the half-life of *SNAI2* mRNA compared with control (siNC; **Fig. 5G**). These data proposed that m6A demethylase ALKBH5 can protect *SNAI2* mRNA stability partially from the YTHDF2-dependent mRNA decay via an m6A demethylation manner.

To further explore the accurately m6A methylate site, we first confirmed the binding between ALKBH5 protein and *SNAI2* transcripts by RNA-binding protein immunoprecipitation (RIP). The binding enrichment of P1 region of *SNAI2* mRNA was higher than P2 region while both regions significantly enriched compared with IgG control because the *SNAI2* transcript was not fragmented in the process of RIP (**Fig. 5H**). This ALKBH5-binding difference between the two regions suggested that there may be some structural folds in P2

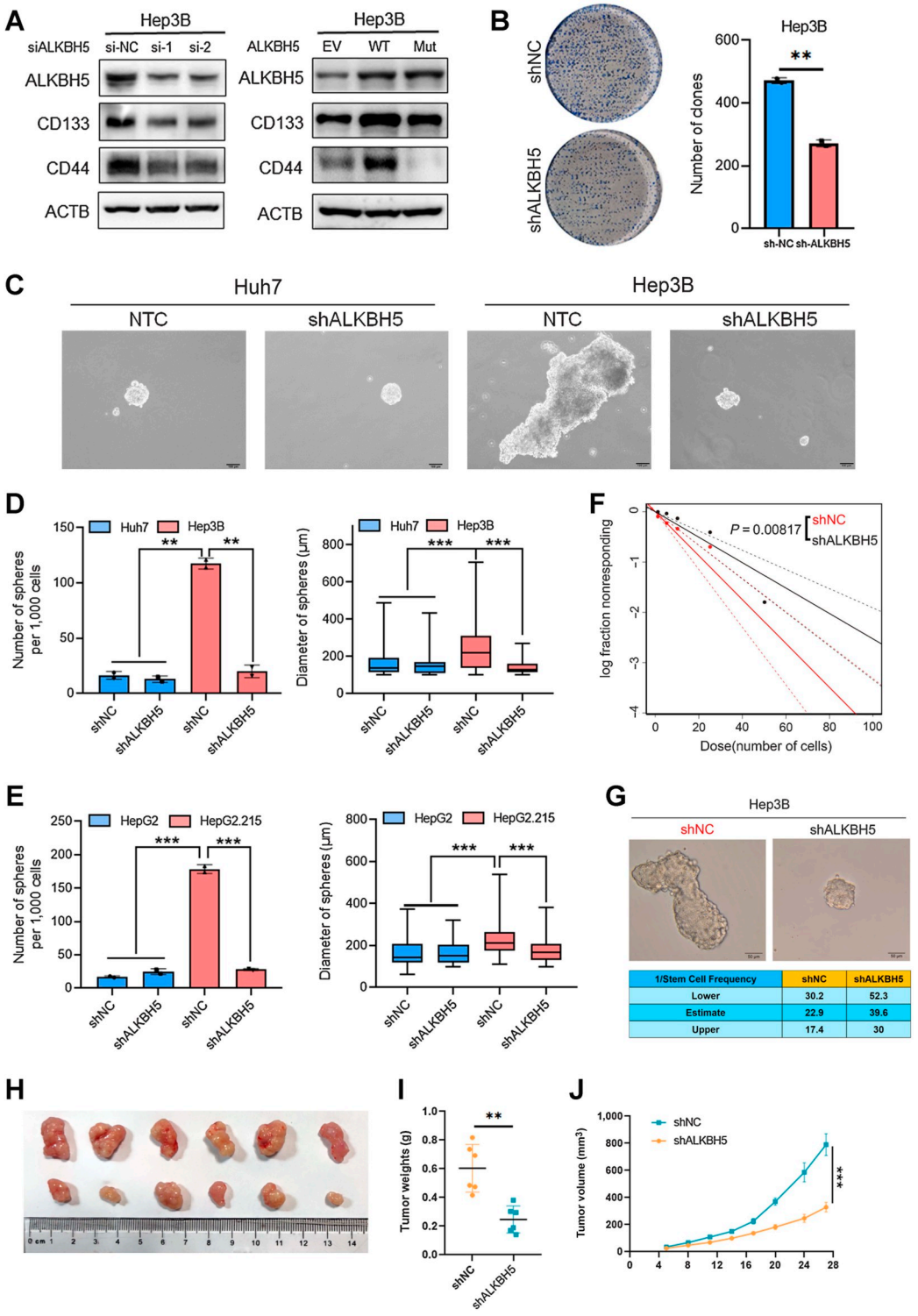

Figure 3.

ALKBH5 is required for the maintenance of hepatoma cell self-renewal in HBV-positive HCC. **A,** ALKBH5, CD133, and CD44 protein expression was identified in ALKBH5-deficient Hep3B cells and ALKBH5-overexpression Hep3B cells through transfected with WT ALKBH5 and m6A methylase activity site mutated ALKBH5 (Mut). siALKBH5; transient siRNA segment against ALKBH5. **B,** Tumor growth of Hep3B cells with or without ALKBH5 knockdown was evaluated by colony formation assay. **C,** Representative images of sphere formation in Huh7 cells and Hep3B cells with or without ALKBH5 knockdown. Scale bar, 100 μm. **D** and **E,** Statistical analysis was performed to quantify the diameter and number of spheres in HepG2, HepG2.215, Huh7, and Hep3B cells with or without ALKBH5 deficient. Spheres were counted from three replicate wells. **F,** Extreme limiting dilution assay (ELDA) was performed in Hep3B cells with ALKBH5 knockdown compared with control and the representative sphere images are shown in **G.** Scale bars, 100 μm. The stemness frequency illustration of the cells with the upper and lower 95% confidence intervals was statistic in **G**. Spheres were counted from 24 replicate wells. **H–J,** Immunodeficient mice ($n = 6$ each group) were subcutaneously inoculated with Hep3B cells treated with endogenous ALKBH5 knockdown, and tumor weights and volumes were monitored. Data are shown as means ± SD; *, $P < 0.05$; **, $P < 0.01$; ***, $P < 0.001$.

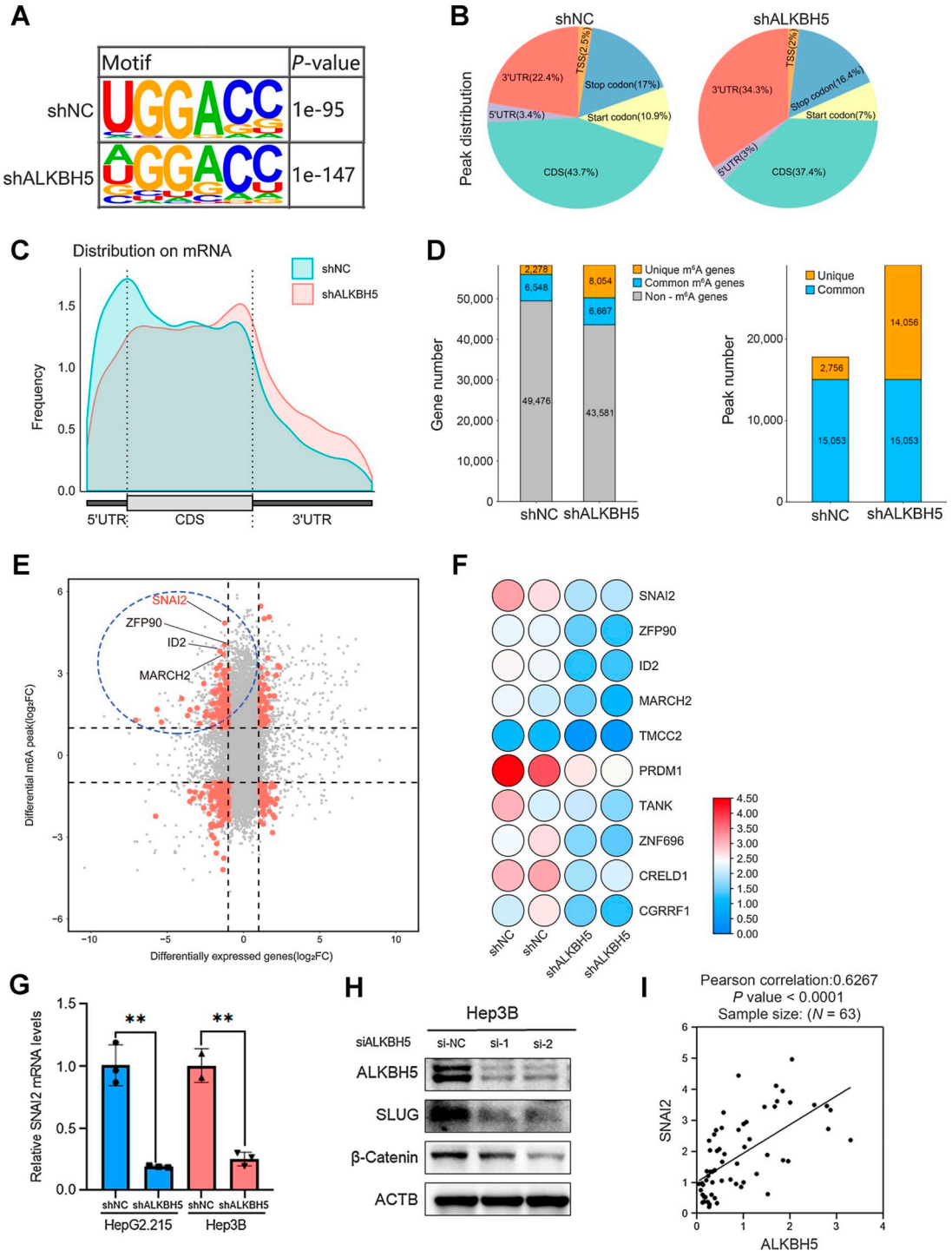

Figure 4.

SNAI2 is a functionally important target gene of ALKBH5 in HBV-positive HCC. **A,** The top enriched motif within m6A peaks were identified in Hep3B cells with or without ALKBH5 knockdown. **B,** Pie charts showing the m6A peak distribution in different regions of RNA transcripts (CDS, start codon, stop codon, TSS, 3′ UTR and 5′ UTR) in Hep3B cells. **C,** Distribution of m6A sites along the length of mRNA transcripts. **D,** Number of m6A-modified genes identified in m6A-seq (left). Number of m6A peaks identified in m6A-seq in Hep3B cells with or without ALKBH5 deficient (right). **E,** MeRIP followed by RNA-seq analysis to identify ALKBH5-mediated RNA methylation and regulation. The correlation between $\log_2$ fold change (FC) of differentially expressed transcripts and $\log_2$ FC of differentially m6A methylated transcripts in Hep3B cells with ALKBH5 knockdown was shown as Volcano plots. **F,** Heat map exhibits the top 10 demethylated genes between control cells and ALKBH5 knockdown cells. **G,** The mRNA expression of *SNAI2* in HepG2.215 and Hep3B cells with ALKBH5-deficient compared with control. **H,** ALKBH5, SLUG and β-catenin protein expression was identified in ALKBH5-deficient Hep3B cells. **I,** A positive correlation between ALKBH5 expression and *SNAI2* expression in HCC patient samples (Pearson correlation = 0.6267, *P* value < 0.0001). Data are shown as means ± SD; $n = 3$; *, $P < 0.05$; **, $P < 0.01$; ***, $P < 0.001$.

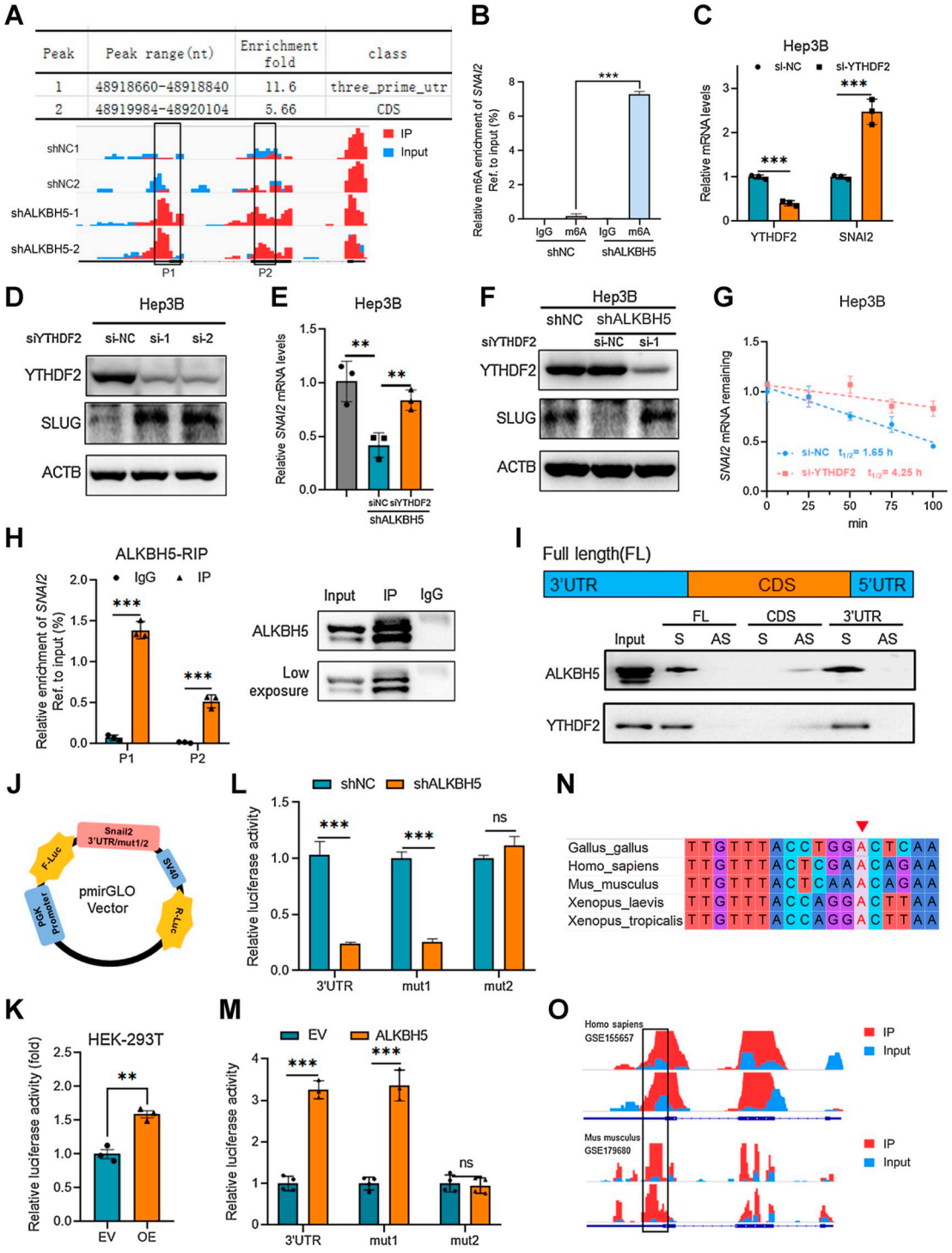

Figure 5.

ALKBH5-mediated m6A demethylation in 3′ UTR stabilizes *SNAI2* mRNA via an YTHDF2-dependent pathway. **A,** IGV plot containing tracks for m6A-seq IP reads (red) and input reads (blue) at *SNAI2* transcript. The sequence of m6A peak is highlighted in two black boxes. **B,** meRIP-qPCR was used to quantify relative SNAI2 peak1 m6A levels in Hep3B cells. **C** and **D,** The mRNA and protein expression of YTHDF2 and SNAI2 in Hep3B cells with YTHDF2 knockdown. **E** and **F,** The mRNA and protein expression of YTHDF2 and SNAI2 in ALKBH5-deficient Hep3B cells with or without downregulation of indicated YTHDF2. **G,** Stability of SNAI2 mRNA in YTHDF2-knockdown Hep3B cells. **H,** Relative enrichment of SNAI2 RNA interact with ALKBH5 protein was identified by RIP assays using anti-IgG (negative control) and anti-ALKBH5 antibodies. **I,** Proteins lysate in Hep3B cells pulled down by the indicated biotin-RNAs were analyzed with ALKBH5 and YTHDF2 antibodies. S, sense, AS, antisense. **J,** Graphical explanation for construction of luciferase reporters. The WT or mutant sequence (mut1 and mut2) of SNAI2 3′ UTR was inserted into pmirGLO vector between Firefly and *Renilla* elements. **K,** Relative luciferase activity of HEK293 cells transfected with *SNAI2* WT luciferase vector was measured. **L** and **M,** Relative luciferase activity of SNAI2 in ALKBH5-deficient Hep3B cells and ALKBH5-upregulated Hep3B cells transfected with WT luciferase vector, Mut1 vector, and Mut2 vector were identified. **N,** Diagram of conserved sequences of *SNAI2* genes from various organisms. The conserved sites are indicated by red typeface. **O,** m6A-seq reads cluster at the same distinct regions of SNAI2 in both human RNA (top) and mouse RNA (bottom) by analyzing meRIP-seq data (GSE155657 and GSE179680). Data are shown as means ± SD; $n = 3$; *, $P < 0.05$; **, $P < 0.01$; ***, $P < 0.001$.

region while P1 region is more likely to be exposed for relevant mRNA modifications. RNA pulldown assay was performed and the results showed that the 3′ UTR fragment of *SNAI2* mRNA pulled down both ALKBH5 protein and YTHDF2 protein from Hep3B cell lysates (**Fig. 5I**). All together, these findings suggested that both YTHDF2 and ALKBH5 bind to the 3′ UTR of *SNAI2* transcripts to affect its stability.

To search for the essential regulatory site of *SNAI2* mRNA, we designed a luciferase reporter plasmid by inserting pmirGLO vector with a WT 3′ UTR sequence of *SNAI2* or mutant (Mut1/Mut2) counterpart putative in which m6A sites were mutated from adenosine to cytosine (**Fig. 5J**; Supplementary Fig. S4D). The HEK293T cells cotransfected with ALKBH5 plasmid and 3′ UTR of *SNAI2* (WT) plasmid exhibited higher luciferase activity than control cells with EV (**Fig. 5K**). The luciferase activity of Hep3B cells transfected with *SNAI2*-3′ UTR-WT plasmid tended to decrease when knocking down ALKBH5 (**Fig. 5L**) and tended to elevate when ALKBH5 was overexpressed (**Fig. 5M**), while that of Mut2 group but not Mut1 group seemed to be unaffected (**Fig. 5L** and **M**). Moreover, examination of the sequence of *SNAI2* 3′ UTR transcript revealed that the m6A adenosine in site2 (Mut2) of *SNAI2* mRNA is highly conserved across species (**Fig. 5N**). The m6A peaks were visualized to be enriched near site2 (mut2) in the 3′ UTR of *SNAI2* in both human and murine livers by analyzing the published MeRIP-seq data (**Fig. 5O**). Taken together, our findings demonstrated that ALKBH5-mediated m6A demethylation on the 3′ UTR of *SNAI2* transcripts enhanced its mRNA stability in HBV-positive HCC by preventing YTHDF2-dependent mRNA decay.

SLUG is involved in ALKBH5-regulated stem-like properties of HBV-related HCC

We next evaluated the effects of SLUG/*SNAI2* in the regulation of ALKBH5-mediated cancer stem–like phenotypes of HBV-positive HCC. The SLUG protein level and mRNA expression of *SNAI2* were elevated in HBV-positive HCC tissues compared with HBV-negative HCC (**Fig. 6A** and **B**). In addition, forced expression of *SNAI2* could reverse the expression of stemness factors (Supplementary Fig. S5A–S5D) and remarkably restored sphere formation ability in endogenous ALKBH5-depleted Hep3B cells (shALKBH5-*SNAI2*) using extreme limiting dilution assays and replanting sphere formation assays (**Fig. 6C**–**E**). Endogenous ALKBH5 stably knockdown cells with forced expression of *SNAI2* (shALKBH5-*SNAI2*) or EV (shALKBH5-EV) and control cells (shNC) were injected into nude mice to form tumor separately. Mice inoculated with cells overexpressing SLUG (shALKBH5-*SNAI2*) significantly rescued the volume of tumor masses compared with the mice injected with ALKBH5-deficient cells (shALKBH5-EV; **Fig. 6F**; Supplementary Fig. S5E). To investigate the oncogenic function of ALKBH5/*SNAI2* in more closely mimics of the clinical situations, we established human primary HCC-derived organoid culture with or without stably altered ALKBH5 and *SNAI2* expression (**Fig. 6G** and **H**). ALKBH5 knockdown resulted in decreased number and diameter of organoids and *SNAI2* overexpression reversed this phenotype (**Fig. 6I** and **J**). The expressions of CSC-related biomarker were downregulated in ALKBH5 knockdown organoids while SNAI2 overexpression showed the opposite effects (Supplementary Fig. S5F). In conclusion, *SNAI2* is a bona fide functionally significant target of ALKBH5 in HBV-related HCC. The ALKBH5-*SNAI2* axis contributes to the stem cell properties of HBV-positive HCC.

ALKBH5/*SNAI2* axis promotes tumor immune evasion by regulating CD155

Immune checkpoint blockade exhibits considerable potential in immunotherapy in malignancies. HCC stem cell reported to be regulated by the microenvironment and escape immune attack (29, 30). We speculated that ALKBH5/SNAI2 axis may enhancing tumor immune escape. We detected the expression of immune checkpoint ligands CD274, CD80, CD155, and CD112 in Hep3B and HepG2.215 stable cell lines, the result show that CD155 was positively regulated by ALKBH5/SNAI2 axis (**Fig. 7A**; Supplementary Fig. S5G–S5I). Similar results were obtained in sphere formation and organoids samples (**Fig. 7B** and **C**). In addition, we observed a positive correlation between CD155 and ALKBH5/SNAI2 in HCC tumor samples (**Fig.7D**). CD155 had been identified as a common ligand which transmit inhibitory signals from TIGIT therewith inhibit natural killer (NK)-mediated tumor killing functions (31). Several evidences have suggested that NK cell in HCC tumor show significant reduction and functionally exhausted with impaired cytotoxicity (32). We determined oncolysis using RTCA system. Hep3B and HepG2.215 with deplete ALKBH5 coculture with NK-92 MI cells led to enhanced tumor cell destruction compared with control (**Fig. 7E** and **F**).

Further analysis of murine-derived CD3-NK1.1+ cells with additional representative markers revealed that knockdown ALKBH5 promotes NK1.1+ NK cell function with increased levels of cytokines including granzyme B and IFNγ and SNAI2 overexpression reversed this elevation (**Fig. 7G** and **H**). Taken together, ALKBH5/SNAI2 promotes the expression of CD155 and increases immune escape of HCC in NK-mediated tumor killing. This study revealed that HBV mediated the downregulation of m6A by stabilized ALKBH5 mRNA, which enhanced the expression of SNAI2 and promote the stemness maintenance of HCC. ALKBH5/SNAI2 axis accelerates the immune escape of HCC to NK cell–mediated tumor killing.

Discussion

Chronic HBV infection is the most predominant etiology of HCC (33, 34). And HCC has been identified as a complex and heterogeneous disease (35, 36). The treatment resistance in immunotherapy of liver CSCs remains to be explored. HBV has been reported to promote the CSC properties, migration, invasion, proliferation, and sorafenib resistance of HCC cells (37–39). Thus, searching and targeting the key oncogene to eradicate CSCs is crucial to hinder HCC. In our study, we demonstrated an oncogenic function of ALKBH5 to stabilize *SNAI2* mRNA through reducing the m6A modification in 3′ UTR in HBV-positive HCC. Interestingly, *SNAI2* has been shown to contribute to the stem-like cell maintenance and self-renewal in HCC (40) and breast cancer (27). Indeed, inhibition of ALKBH5 suppresses stem-like cell properties which is reversed by upregulation of *SNAI2*. We here unveiled the role of ALKBH5-mediated m6A demethylation in stabilizing *SNAI2* transcript and identified a significant oncogenic function of ALKBH5 in promoting the CSC phenotype of HBV-related HCC.

Accumulating lines of evidence have revealed the mechanisms responsible for the dysregulation of m6A modification in cancer and virus infection–related innate immune response (41). Another study reported that there is a positive-feedback loop between HBx and ALKBH5 to promote the tumor progression of HCC (42). HBx also be identified as an oncogene which induces stem-like cell features in HCC (12, 43). And we previously demonstrated that HBV protein P (HBp) initiates glycolytic bypass and promote tumor progression in HBV-related HCC (24). In this study, we found that the

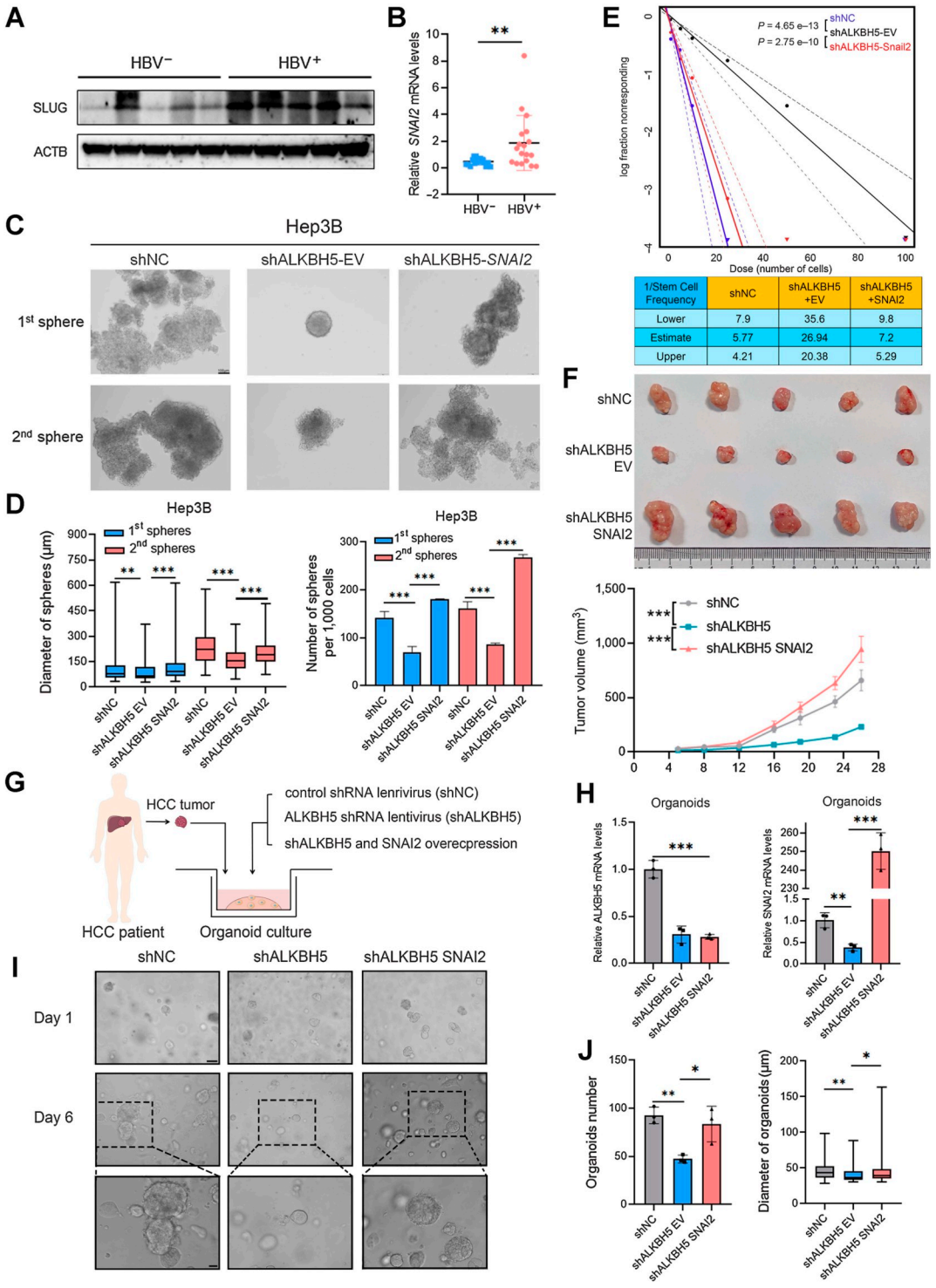

Figure 6.

SNAI2 is a functionally important target gene of ALKBH5 in HBV-positive HCC. **A** and **B,** The protein and mRNA expressions of SNAI2 in HBV-negative and HBV-positive HCC tissues. **C** and **D,** Replanting sphere formation was performed in Hep3B cells with endogenous ALKBH5 knockdown and forced expression of indicated SNAI2. The represent images were shown in **C**. Scale bar, 100 μm. The diameter and number of spheres were quantified from three replicate wells. **E,** Extreme limiting dilution assay (ELDA) was addressed in Hep3B cells with ALKBH5 knockdown and forced expression of SNAI2. Stemness frequency illustration of the cells with the upper and lower 95% confidence intervals meaning that the frequency of one stem cell in cancer cells ($n = 24$). **F,** Immunodeficient mice ($n = 5$, biological replicates each group) were subcutaneously inoculated with Hep3B cells with ALKBH5 knockdown and forced expression indicated SNAI2, and tumor volumes were monitored. **G,** HCC organoid culture was performed as indicated in the schematic diagram. **H,** qRT-PCR analysis of ALKBH5 and SNAI2 expression levels in organoids with or without lentiviral vectors infection. **I,** Representative images of HCC organoids after infection with indicated lentiviral vectors: shNC, shALKBH5, and shALKBH5 with SNAI2 overexpression. Scale bar, 50 μm. **J,** The diameter and number of organoids were quantified from three replicate wells. Data are shown as means ± SD; $n = 3$; *, $P < 0.05$; **, $P < 0.01$; ***, $P < 0.001$.

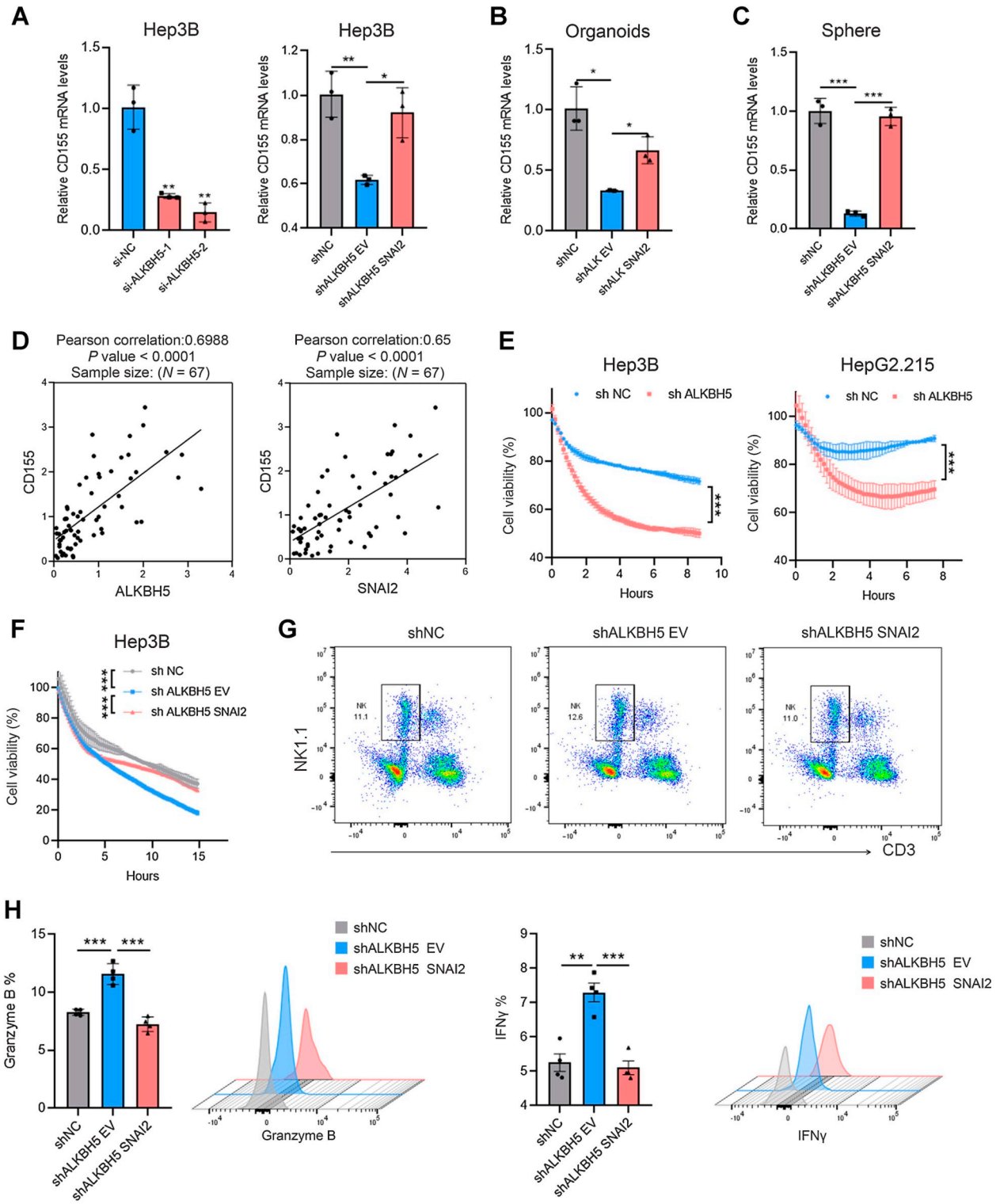

Figure 7.

ALKBH5/*SNAI2* axis promotes tumor immune evasion by regulating CD155. **A,** Relative mRNA levels of CD155 in Hep3B and HepG2.215 transfected with siRNA segment target to ALKBH5 and in Hep3B stable lines with endogenous ALKBH5 knockdown and forced expression of indicated SNAI2. **B,** The expression of CD155 in organoids with endogenous ALKBH5 knockdown and forced expression of indicated SNAI2. **C,** The expression of CD155 in spheres performed from Hep3B cells with lentiviral vectors infection. **D,** The positive correlation between ALKBH5/SNAI2 expression and CD155 expression in HCC patient samples. **E,** The cell viability was analyzed using RTCA in Hep3B and HepG2.215 stable cell lines with ALKBH5 knockdown (sh ALK). **F,** Cell viability was assessed in Hep3B stable lines with endogenous ALKBH5 knockdown and forced expression of indicated SNAI2. **G** and **H,** Flow cytometry–based quantification of granzyme B–positive cells and IFNγ-positive cells among NK1.1+ NK cells after *in vitro* stimulation with phorbol myristate acetate, Brefeldin A, and ionomycin ($n = 4$). Data are shown as means ± SD; *, $P < 0.05$; **, $P < 0.01$; ***, $P < 0.001$.

upregulation effect of HBV infection on ALKBH5 was much higher than that of transfected with HBV-related proteins. HBV stabilizes the mRNA of ALKBH5, which subsequently decreases the m6A level and elevates stemness traits in HBV-positive HCC. Because ALKBH5 was reported to suppress the tumor progression of HCC (44) and the stemness properties were attenuated by knocking down ALKBH5 only in HBV-positive HCC but not HBV-negative HCC. We speculated that this phenotype may have something to do with specific cell conditions. We believe that enhancing ALKBH5 stability is not the only function of HBV in the m6A-mediated regulation of self-renewal in HBV-related HCC.

Recent study has shown that m6A modification relevant to antitumor immunity and the reader YTHDF1 promote an immunosuppressive tumor microenvironment to accelerate the tumorigenesis of colorectal cancer (45). In our study, ALKBH5 and SNAI2 regulated the escape of HCC in NK-mediated tumor killing. Given that chronic HBV infection alter the immune microenvironment of HCC, subsequent research should focus on the relationship of HBV-mediate m6A hypermethylation and antitumor immunity (46).

Collectively, our results revealed that ALKBH5 interacts with 3′ UTR of *SNAI2* transcripts to demethylated m6A modification further enhanced the stability of *SNAI2* to maintain its high expression and contribute to the stemness phenotype and immune escape of HBV-related HCC. Precisely targeting the expression of ALKBH5 is critical for the therapeutic approach for HBV-related HCC.

Authors' Disclosures

No disclosures were reported.

Authors' Contributions

Y. Meng: Conceptualization, data curation, formal analysis, supervision, validation, investigation, visualization, methodology, writing–original draft, project administration, writing–review and editing. **Z. Shu:** Resources, Data curation, methodology. **X. Wang:** Data curation, methodology. **L. Hong:** Data curation, validation, investigation, methodology. **B. Wang:** Resources. **J. Jiang:** Data curation, investigation. **K. He:** Data curation, methodology. **Q. Cao:** Data curation, software, methodology. **F. Shi:** Data curation, investigation. **H. Wang:** Software, writing–review and editing. **L. Gong:** Investigation, writing–review and editing. **H. Diao:** Conceptualization, supervision, funding acquisition, investigation, project administration, writing–review and editing.

Acknowledgments

National Key Research and Development Program of China (2021YFA1301100, 2021YFA1301101), The Fundamental Research Funds for the Central Universities (2022ZFJH003), Research Project of Jinan Microecological Biomedicine Shandong Laboratory (JNL-2022012B, JNL-2022043D), Public Welfare Foundation of Zhejiang Science and Technology Agency (no. LGF22H160047).

Note

Supplementary data for this article are available at Molecular Cancer Research Online (http://mcr.aacrjournals.org/).

Received January 7, 2024; revised February 22, 2024; accepted March 26, 2024; published first March 28, 2024.

References

1. Yang JD, Hainaut P, Gores GJ, Amadou A, Plymoth A, Roberts LR. A global view of hepatocellular carcinoma: trends, risk, prevention and management. Nat Rev Gastroenterol Hepatol 2019;16:589–604.
2. Siegel RL, Miller KD, Jemal A. Cancer statistics, 2017. CA Cancer J Clin 2017;67:7–30.
3. Levrero M, Zucman-Rossi J. Mechanisms of HBV-induced hepatocellular carcinoma. J Hepatol 2016;64:S84–S101.
4. Gingold JA, Zhu D, Lee DF, Kaseb A, Chen J. Genomic profiling and metabolic homeostasis in primary liver cancers. Trends Mol Med 2018;24:395–411.
5. Jia L, Gao Y, He Y, Hooper JD, Yang P. HBV induced hepatocellular carcinoma and related potential immunotherapy. Pharmacol Res 2020;159:104992.
6. Ma XL, Hu B, Tang WG, Xie SH, Ren N, Guo L, et al. CD73 sustained cancer-stem-cell traits by promoting SOX9 expression and stability in hepatocellular carcinoma. J Hematol Oncol 2020;13:11.
7. Craig AJ, von Felden J, Garcia-Lezana T, Sarcognato S, Villanueva A. Tumour evolution in hepatocellular carcinoma. Nat Rev Gastroenterol Hepatol 2020;17:139–52.
8. Xu C, Jin G, Wu H, Cui W, Wang YH, Manne RK, et al. SIRPgamma-expressing cancer stem-like cells promote immune escape of lung cancer via Hippo signaling. J Clin Invest 2022;132:e141797.
9. Gao Y, You M, Fu J, Tian M, Zhong X, Du C, et al. Intratumoral stem-like CCR4+ regulatory T cells orchestrate the immunosuppressive microenvironment in HCC associated with hepatitis B. J Hepatol 2022;76:148–59.
10. Zhang C, Li J, Cheng Y, Meng F, Song JW, Fan X, et al. Single-cell RNA sequencing reveals intrahepatic and peripheral immune characteristics related to disease phases in HBV-infected patients. Gut 2023;72:153–67.
11. Fan H, Zhang H, Pascuzzi PE, Andrisani O. Hepatitis B virus X protein induces EpCAM expression via active DNA demethylation directed by RelA in complex with EZH2 and TET2. Oncogene 2016;35:715–26.
12. Arzumanyan A, Friedman T, Ng IO, Clayton MM, Lian Z, Feitelson MA. Does the hepatitis B antigen HBx promote the appearance of liver cancer stem cells? Cancer Res 2011;71:3701–8.
13. Chen M, Wong CM. The emerging roles of N6-methyladenosine (m6A) deregulation in liver carcinogenesis. Mol Cancer 2020;19:44.
14. Visvanathan A, Patil V, Arora A, Hegde AS, Arivazhagan A, Santosh V, et al. Essential role of METTL3-mediated m(6)A modification in glioma stem-like cells maintenance and radioresistance. Oncogene 2018;37:522–33.
15. Vu LP, Pickering BF, Cheng Y, Zaccara S, Nguyen D, Minuesa G, et al. The N(6)-methyladenosine (m(6)A)-forming enzyme METTL3 controls myeloid differentiation of normal hematopoietic and leukemia cells. Nat Med 2017;23:1369–76.
16. Barbieri I, Tzelepis K, Pandolfini L, Shi J, Millan-Zambrano G, Robson SC, et al. Promoter-bound METTL3 maintains myeloid leukaemia by m(6)A-dependent translation control. Nature 2017;552:126–31.
17. Jia G, Fu Y, Zhao X, Dai Q, Zheng G, Yang Y, et al. N6-methyladenosine in nuclear RNA is a major substrate of the obesity-associated FTO. Nat Chem Biol 2011;7:885–7.
18. Li Z, Weng H, Su R, Weng X, Zuo Z, Li C, et al. FTO Plays an oncogenic role in acute myeloid leukemia as a N(6)-methyladenosine RNA demethylase. Cancer Cell 2017;31:127–41.
19. Peng F, Xu J, Cui B, Liang Q, Zeng S, He B, et al. Oncogenic AURKA-enhanced N(6)-methyladenosine modification increases DROSHA mRNA stability to transactivate STC1 in breast cancer stem-like cells. Cell Res 2021;31:345–61.
20. Zhang Y, Liu X, Wang Y, Lai S, Wang Z, Yang Y, et al. The m(6)A demethylase ALKBH5-mediated upregulation of DDIT4-AS1 maintains pancreatic cancer stemness and suppresses chemosensitivity by activating the mTOR pathway. Mol Cancer 2022;21:174.
21. Zhu Z, Hao X, Yan M, Yao M, Ge C, Gu J, et al. Cancer stem/progenitor cells are highly enriched in CD133+CD44+ population in hepatocellular carcinoma. Int J Cancer 2010;126:2067–78.
22. Gao X, Sheng Y, Yang J, Wang C, Zhang R, Zhu Y, et al. Osteopontin alters DNA methylation through up-regulating DNMT1 and sensitizes CD133+/CD44+ cancer stem cells to 5 azacytidine in hepatocellular carcinoma. J Exp Clin Cancer Res 2018;37:179.
23. Hou Y, Zou Q, Ge R, Shen F, Wang Y. The critical role of CD133(+) CD44(+/high) tumor cells in hematogenous metastasis of liver cancers. Cell Res 2012;22:259–72.
24. Chen W, Jiang J, Gong L, Shu Z, Xiang D, Zhang X, et al. Hepatitis B virus P protein initiates glycolytic bypass in HBV-related hepatocellular carcinoma via a FOXO3/miRNA-30b-5p/MINPP1 axis. J Exp Clin Cancer Res 2021;40:1.
25. Li X, Zhang Y, Wang J, Li Y, Wang Y, Shi F, et al. zVAD alleviates experimental autoimmune hepatitis in mice by increasing the sensitivity of macrophage to TNFR1-dependent necroptosis. J Autoimmun 2022;133:102904.

26. Yao C, Su L, Shan J, Zhu C, Liu L, Liu C, et al. IGF/STAT3/NANOG/slug signaling axis simultaneously controls epithelial-mesenchymal transition and stemness maintenance in colorectal cancer. Stem Cells 2016;34:820–31.
27. Zhou L, Wang D, Sheng D, Xu J, Chen W, Qin Y, et al. NOTCH4 maintains quiescent mesenchymal-like breast cancer stem cells via transcriptionally activating SLUG and GAS1 in triple-negative breast cancer. Theranostics 2020; 10:2405–21.
28. Du H, Zhao Y, He J, Zhang Y, Xi H, Liu M, et al. YTHDF2 destabilizes m(6)A-containing RNA through direct recruitment of the CCR4-NOT deadenylase complex. Nat Commun 2016;7:12626.
29. Wei Y, Shi D, Liang Z, Liu Y, Li Y, Xing Y, et al. IL-17A secreted from lymphatic endothelial cells promotes tumorigenesis by upregulation of PD-L1 in hepatoma stem cells. J Hepatol 2019;71:1206–15.
30. Jia H, Chen J, Zhang X, Bi K, Zhou H, Liu T, et al. IL-17A produced by invariant natural killer T cells and CD3(+) CD56(+) alphaGalcer-CD1d tetramer(-) T cells promote liver fibrosis in patients with primary biliary cholangitis. J Leukoc Biol 2022;112:1079–87.
31. Freed-Pastor WA, Lambert LJ, Ely ZA, Pattada NB, Bhutkar A, Eng G, et al. The CD155/TIGIT axis promotes and maintains immune evasion in neoantigen-expressing pancreatic cancer. Cancer Cell 2021;39:1342–60.
32. Sun H, Huang Q, Huang M, Wen H, Lin R, Zheng M, et al. Human CD96 correlates to natural killer cell exhaustion and predicts the prognosis of human hepatocellular carcinoma. Hepatology 2019;70:168–83.
33. Ding WB, Wang MC, Yu J, Huang G, Sun DP, Liu L, et al. HBV/pregenomic RNA increases the stemness and promotes the development of HBV-related HCC through reciprocal regulation with insulin-like growth factor 2 mRNA-binding protein 3. Hepatology 2021;74:1480–95.
34. Du W, Chen W, Shu Z, Xiang D, Bi K, Lu Y, et al. Identification of prognostic biomarkers of hepatocellular carcinoma via long noncoding RNA expression and copy number alterations. Epigenomics 2020;12:1303–15.
35. Yang H, Ni HM, Ding WX. The double-edged sword of MTOR in autophagy deficiency induced-liver injury and tumorigenesis. Autophagy 2019;15:1671–3.
36. Lee TK, Guan XY, Ma S. Cancer stem cells in hepatocellular carcinoma - from origin to clinical implications. Nat Rev Gastroenterol Hepatol 2022;19:26–44.
37. Lin X, Li AM, Li YH, Luo RC, Zou YJ, Liu YY, et al. Silencing MYH9 blocks HBx-induced GSK3beta ubiquitination and degradation to inhibit tumor stemness in hepatocellular carcinoma. Signal Transduct Target Ther 2020;5:13.
38. Phi LTH, Sari IN, Yang YG, Lee SH, Jun N, Kim KS, et al. Cancer stem cells (CSCs) in drug resistance and their therapeutic implications in cancer treatment. Stem Cells Int 2018;2018:5416923.
39. Liu T, Diao H. A double-edged sword: the HBV-induced non-coding RNAs alterations in hepatocellular carcinoma. Biocell 2023;47:27–32.
40. Tang B, Qi G, Tang F, Yuan S, Wang Z, Liang X, et al. Aberrant JMJD3 expression upregulates slug to promote migration, invasion, and stem cell-like behaviors in hepatocellular carcinoma. Cancer Res 2016;76:6520–32.
41. Winkler R, Gillis E, Lasman L, Safra M, Geula S, Soyris C, et al. m(6)A modification controls the innate immune response to infection by targeting type I interferons. Nat Immunol 2019;20:173–82.
42. Qu S, Jin L, Huang H, Lin J, Gao W, Zeng Z. A positive-feedback loop between HBx and ALKBH5 promotes hepatocellular carcinogenesis. BMC Cancer 2021; 21:686.
43. Wang X, Oishi N, Shimakami T, Yamashita T, Honda M, Murakami S, et al. Hepatitis B virus X protein induces hepatic stem cell-like features in hepatocellular carcinoma by activating KDM5B. World J Gastroenterol 2017;23: 3252–61.
44. Chen Y, Zhao Y, Chen J, Peng C, Zhang Y, Tong R, et al. ALKBH5 suppresses malignancy of hepatocellular carcinoma via m(6)A-guided epigenetic inhibition of LYPD1. Mol Cancer 2020;19:123.
45. Hou J, Zhang H, Liu J, Zhao Z, Wang J, Lu Z, et al. YTHDF2 reduction fuels inflammation and vascular abnormalization in hepatocellular carcinoma. Mol Cancer 2019;18:163.
46. Bao Y, Zhai J, Chen H, Wong CC, Liang C, Ding Y, et al. Targeting m(6)A reader YTHDF1 augments antitumour immunity and boosts anti-PD-1 efficacy in colorectal cancer. Gut 2023;72:1497–509.